Permanent bending and alignment of ZnO nanowires

2011 Nanotechnology 22 185307

(http://iopscience.iop.org/0957-4484/22/18/185307)

Nanotechnology **22** (2011) 185307 (9pp) doi:10.1088/0957-4484/22/18/185307

Permanent bending and alignment of ZnO nanowires

Christian Borschel[1,6], Susann Spindler[1,6], Damiana Lerose[2,3], Arne Bochmann[3], Silke H Christiansen[3,4], Sandor Nietzsche[5], Michael Oertel[1] and Carsten Ronning[1]

[1] Institute for Solid State Physics, Friedrich-Schiller-University Jena, Max-Wien-Platz 1, 07743 Jena, Germany
[2] Max Planck Institute of Microstructure Physics, Weinberg 2, 06120 Halle (Saale), Germany
[3] Institute of Photonic Technology, Albert-Einstein-Strasse 9, 07745 Jena, Germany
[4] Max Planck Institute for the Science of Light, Günther-Scharowsky-Straße 1, 91058 Erlangen, Germany
[5] Centre of Electron Microscopy, Friedrich-Schiller-University Jena, Ziegelmühlenweg 1, 07743 Jena, Germany

E-mail: christian.borschel@uni-jena.de, susann.spindler@uni-jena.de and carsten.ronning@uni-jena.de

Received 16 October 2010, in final form 1 March 2011
Published 22 March 2011
Online at stacks.iop.org/Nano/22/185307

Abstract
Ion beams can be used to permanently bend and re-align nanowires after growth. We have irradiated ZnO nanowires with energetic ions, achieving bending and alignment in different directions. Not only the bending of single nanowires is studied in detail, but also the simultaneous alignment of large ensembles of ZnO nanowires. Computer simulations reveal how the bending is initiated by ion beam induced damage. Detailed structural characterization identifies dislocations to relax stresses and make the bending and alignment permanent, even surviving annealing procedures.

(Some figures in this article are in colour only in the electronic version)

1. Introduction

Semiconductor nanowires (NWs) have been studied intensely in recent years and many synthesis methods as well as a vast range of applications have been presented [1]. Depending on the growth process used, not all possible shapes, morphologies and directions are possible to achieve during growth. For example, epitaxy relations may limit the possible growth directions. Thus, post-growth methods for control of nanowire morphology, shape and assembly are necessary. A few post-growth alignment methods have been reported, for example the Langmuir–Blodgett technique [2], the blown bubble film approach [3], or the dielectrophoresis method [4]. However, it is necessary to suspend the nanowires in a solution for all these methods.

Ion beams have been used for a long time in semiconductor technology, mostly with the purpose of doping by implantation and thus controlling the electrical properties of semiconductors. However, in combination with semiconductor nanowires, new applications for ion beams have emerged besides doping [5]. For example, ion beams have been used for the (indirect) synthesis of nanowires [6, 7] and focused ion beams have been used to contact nanowires [8], to cut out nanowires from bulk [9], to prestructure growth catalysts before nanowire growth [10], to predetermine branching locations [11], or as an aid for cutting while manipulating single nanowires [12]. However, just recently, a few studies have been presented that used direct ion beam irradiation of existing nanowires with the purpose of controlling their shape, morphology or alignment after growth [13–16]. Since the ion beam methods are applied after growth, they are independent of the nanowire synthesis method. Furthermore, ion beam irradiation offers the advantage of simultaneous manipulation of a large number of nanowires by using broad ion beams.

In a previous paper we have shown that ion beams can be used to bend and align GaAs nanowires [16]. In this paper, we expand the studies to ZnO nanowires, suggesting that the discussed mechanisms are universal for semiconductors and

[6] The first two authors contributed equally to this paper.

not limited to GaAs. However, this report is not only limited to a new material: we present a much more detailed study of the underlying mechanisms by using focused ion beams for irradiation of single nanowires with *in situ* characterization as well as an investigation of the microscopic structure of the bent nanowires. Additionally, we study the persistency of the bending upon annealing, which is mandatory after ion irradiation to restore the crystal quality of semiconductors.

The irradiation experiments were accompanied by Monte Carlo computer simulations. From these, the distribution of implanted ions within the nanowires is determined. Furthermore, the simulations yield the distribution of irradiation damage within the nanowire, which is crucial for understanding the bending and alignment processes.

2. Experimental details

The ZnO nanowires were grown epitaxially on Si substrates coated with ZnO and on AlN substrates. After cleaning the AlN substrates with acetone and isopropanol and drying with nitrogen, they were coated by thermal evaporation with a 5 nm thick gold layer, which served as a catalyst for the nanowire growth. The growth took place in a tube furnace accordant to the vapour–liquid–solid (VLS) growth mechanism [17, 18]. The lattice misfit between AlN and ZnO is $\leqslant 5\%$, which is sufficient to provide epitaxial growth of the nanowires; in fact, tension due to the different lattice constants has no significant impact because the NW cross section is small. The nanowires grew perpendicular to the substrate and were densely arranged.

To produce straight nanowires with different orientations, Si substrates with ZnO buffer layers were used as an alternative to AlN. The need for inclined nanowires arises from geometrical constraints between the nanowire axis and the angles of incidence of the ion beam and electron beam when irradiating nanowires using a focused ion beam (FIB) (see below). The ZnO buffer layers were fabricated by radio frequency magnetron sputter deposition after cleaning the substrates. The nanowires were also grown in a tube furnace, but without catalyst.

By changing the thickness of the polycrystalline ZnO buffer layer it is possible to tune the orientations of the growing nanowires between totally random and uniform perpendicular alignment [19]. This is due to the high growth rate of the (0001)-plane: grains which are oriented with the *c*-axis [0001] perpendicular to the substrate surface grow faster. Therefore, with increasing film thickness, such [0001]-oriented grains becomes the major component forming the ZnO buffer layer while other orientations are suppressed. The ZnO nanowires grow in the *c*-direction as well, hence the major orientation of the buffer layer is transferred to the NWs. For our experiments we have grown perpendicular as well as inclined nanowires.

In order to study how nanowires react to ion beam irradiation, two different groups of experiments have been performed. (1) In the first group, macroscopic samples with a high density of nanowires were irradiated with ion beams of large diameter (about 1 cm). These experiments will be denoted as 'ensemble irradiation' from now on. (2) For the second group of irradiation experiments, focused ion beams were used, whose lateral resolution allows the irradiation of single nanowires; these experiments will be referred to as 'single NW irradiation'.

An implanter (High Voltage Engineering Europa) was used to perform the ensemble irradiation which is capable of accelerating ions of almost any chemical element and ion energies between 10 and 380 keV. This allows one to realize two different irradiation conditions: (A) low energies can be chosen to make the ions stop close to the surface of the nanowires ('shallow implantation'). (B) Higher energies can be selected to implant the ions deep into the NW and let the complete nanowire cross section be affected ('deep implantation').

To study how the nanowire shape evolves with increasing ion fluence (=dose), the samples have to be irradiated in steps of small ion fluence and characterized between every step. Since the characterization of the NW shape is done *ex situ* using a scanning electron microscope (SEM), the samples have to be removed from the implanter, transferred to the SEM, characterized, taken back into the implanter and so forth. This is a time-consuming process allowing only a limited number of fluence-steps to be performed.

This disadvantage is avoided in the second group of experiments, namely single NW irradiation: here we use a Tescan Lyra_{XMU} ($\text{VELA}_{\text{FIBxSEM}}$ 3 XM), which provides a focused ion beam (FIB) and a SEM (thermal tungsten cathode). Inclined nanowires were used in this case, since the irradiation with the ion beam is optimized to be perpendicular to the substrate. When the nanowires are irradiated using the FIB the progress is monitored *in situ* with the SEM.

However, the disadvantage of the FIB with SEM is that the choice of ions is limited to gallium and their energy is limited to a maximum of 30 keV. For most nanowires, this restricts use of the FIB to the situation (1), of shallow implantation. Thus, the first group of ensemble measurements using the general purpose implanter is absolutely necessary to realize deep implantation. Furthermore, as it offers the choice of arbitrary ion species, the influence of chemical effects depending on the element can be studied. In particular, noble gas ions are used to exclude chemical effects as the driving mechanism for the evolution of NW shape during ion beam irradiation. All irradiations were performed at room temperature.

Semiconductors subjected to ion beam irradiation usually need subsequent annealing in order to get rid of the damage and for example activate possible dopants [5, 20]. In order to check the stability of the bending and alignment process against annealing, we annealed bent nanowires in air at ambient pressure and temperatures up to 800 °C for 30 min. This temperature was chosen because from previous results we know that typically 700 °C are required to heal the crystal sufficiently to activate dopants and restore the optical properties after ion beam doping of ZnO NWs [21].

Transmission electron microscopy (TEM) measurements (using a JEOL JEM-3010) were performed in order to investigate the impact of the ion irradiation and the annealing on the crystal structure of the nanowires.

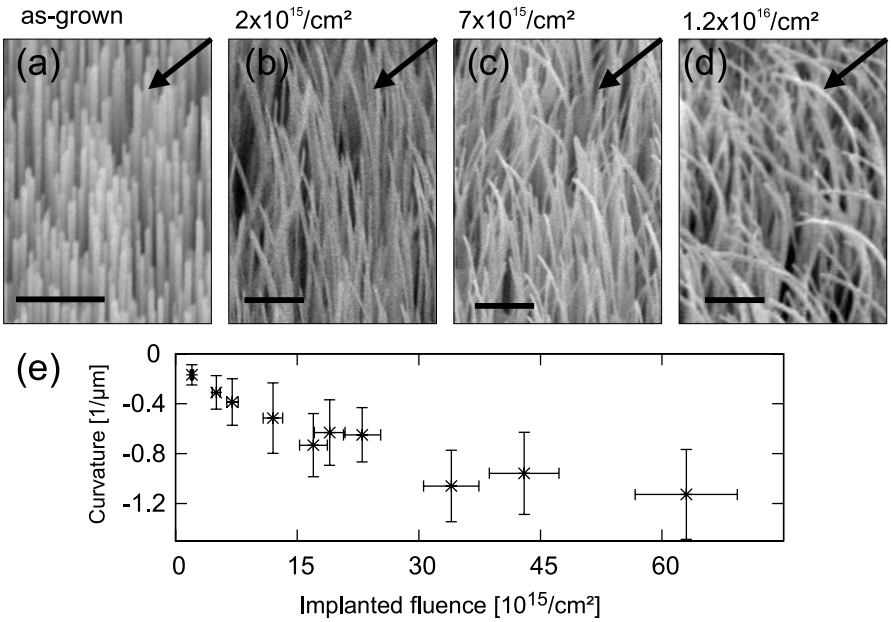

Figure 1. ((a)–(d)) SEM images of nanowires (typically 60 nm diameter) irradiated with increasing fluence of 20 keV Ar ions (low energy situation). Scale bars denote 1 μm. Arrows indicate ion beam direction. (e) Average nanowire curvatures as a function of fluence.

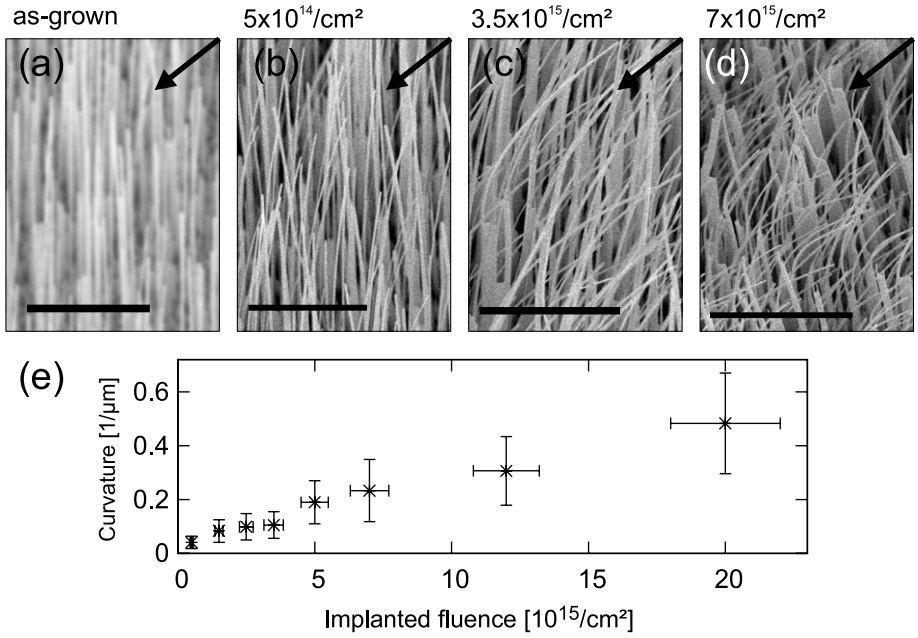

Figure 2. ((a)–(d)) SEM images of nanowires (typically around 90 nm diameter) irradiated with an increasing fluence of 100 keV Ar ions (high energy situation). Scale bars denote 5 μm. Arrows indicate ion beam direction. (e) Average nanowire curvatures as a function of fluence, measured at point of strongest bending.

3. Results and discussion

3.1. Large area ensemble irradiation

For the case of low energy ensemble irradiation (situation (1A)), it can be observed that the nanowires bend away from the incident ion beam. This effect is illustrated in figure 1, which shows a series of SEM images of ZnO nanowires that have been irradiated with an increasing fluence of Ar^+ ions with an energy of 20 keV. The nanowires, which are initially straight and perpendicular, bend towards the left when irradiated with an ion beam under an oblique angle from the right (arrows in figure 1).

The situation is quite different for the case of high energy irradiation (situation (1B)). In that case, the nanowires are observed to bend towards the incident ion beam and align parallel to the ion beam direction. Figure 2 illustrates this process with a series of SEM images recorded after an

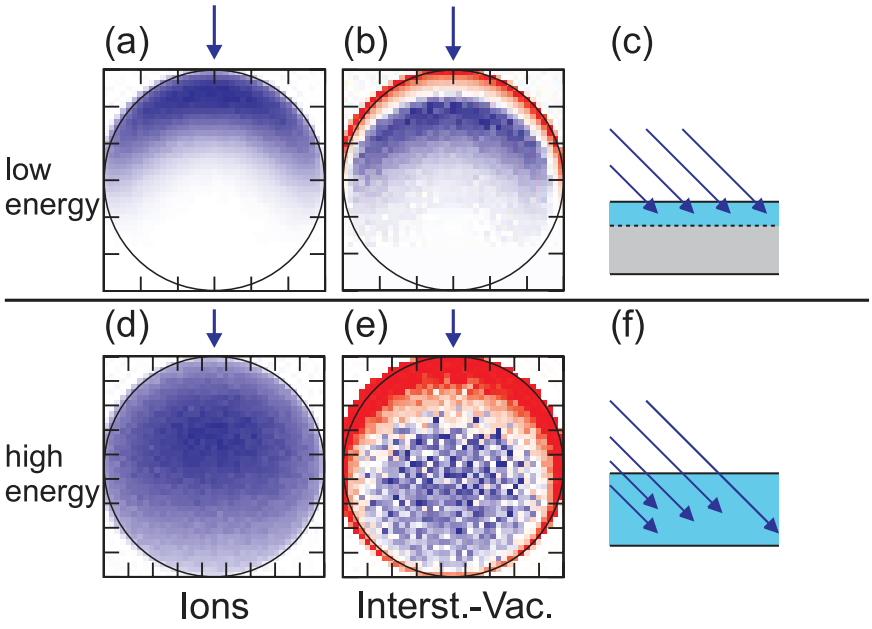

Figure 3. Results of Monte Carlo simulation of ion beam irradiation of ZnO NW. ((a), (b), (d), (e)) Schematic cross sectional view of a NW, irradiated from the top (blue arrows). Top row: 20 keV Ar^+ (shallow implantation, NW diameter 60 nm), bottom row: 100 keV Ar^+ (deep implantation, NW diameter 90 nm). Left column, (a) and (d), shows distribution of implanted ions, centre column, (b) and (e), shows distribution of remaining damage. Red: vacancy excess (grey fringes close to NW surface), blue: interstitial excess (grey area inside NW). Right column, (c) and (f): schematic side view of irradiation.

increasing fluence of irradiation with Ar^+ ions having a higher energy of 100 keV.

For a more quantitative analysis of the bending process, we measured the curvatures of the nanowires after each irradiation step. The curvature is measured from SEM images by matching a circle of radius r to each nanowire and defining the curvature as r^{-1}. The results are shown in figures 1(e) and 2(e), respectively. We use negative values for the curvature to denote bending away from the ion beam and positive values for bending towards the ion beam. A large number of nanowires were measured for each data point; the statistical distribution of the curvatures is denoted by the error bar. The curvature results confirm the qualitative impression from the SEM images: the bending increases with increasing ion fluence for both situations of low and high energy implantation. The nanowires do not all have exactly the same diameter, which accounts for the scatter in the curvature values. Thus, no specific relationship between curvature and implantation fluence can be extracted. More insight is gained from single nanowire irradiation, see section 3.2.

In order to understand these opposite bending processes, one needs to examine the interaction of the ion beam with the nanowire. At the energies used in this study, the ions lose most of their energy in collisions with target nuclei. Target atoms can be displaced from their lattice sites and cause further displacements, leading to a collision cascade. In the conditions used in this study, the number of interstitials and vacancies created per each incoming ion can be on the order of 5×10^3. Thus, the impact of the ion beam damage on the bending is much larger than from the implanted ions themselves. Furthermore, the noble gas atoms can diffuse out of the semiconductor NW, but the bending is permanent and even survives annealing (see below). We conclude that the implanted ions themselves play no major role in the bending process.

Considering the defects, we need to bear in mind that interstitials and vacancies can annihilate each other. In ZnO, a large number of point defects annihilate even far below room temperature [22]; nevertheless, some defects always remain in the crystal.

In order to obtain the distribution of interstitials and vacancies in the irradiated nanowires, we use a Monte Carlo computer code which simulates the transport of ions through matter. Frequently, these simulations are carried out with the widely used SRIM code [23]. However, SRIM only considers flat and layered targets and is therefore not suited very well for simulating the implantation into NWs. Thus, we use the code developed in house called 'iradina', which in principle works similar to SRIM but supports flexible 3D target definitions and can therefore simulate irradiation of nanostructures. (A detailed description of this open source code is in [24].)

In order to limit the necessary simulation volume, we only use a thin disc cut out of the NW and apply periodic boundary conditions in the axial direction. The disc is 10 nm thick, which is sufficiently larger than the free flight length of the ions in the simulation. Perpendicular to the NW axis, the simulation volume is divided into 40×40 cells. The transport of typically 10^6 ions through the nanowire material is simulated and in each cell the number of stopped ions is summed up. Furthermore, the number of vacancies and interstitials created during the ion beam irradiation is summed up in each cell. This procedure allows one to determine the cross sectional distribution of damage and implanted ions in the nanowire.

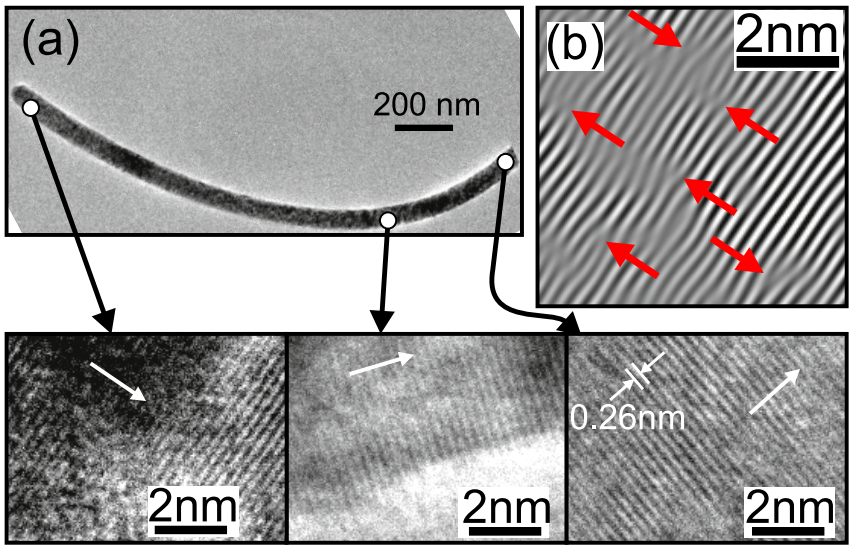

Figure 4. TEM images of a bent nanowire after implantation of 2×10^{16} ions cm^{-2} with 100 keV Ar ions. (a) Overview TEM micrograph and three HR-TEM images taken at different points on the nanowire. The line spacing in the HR-TEM micrographs corresponds to the Zn-plane spacing in the *c*-direction indicated by the white arrows. (b) Fourier-filtered HR-TEM image with arrows pointing to dislocations.

Figure 3 illustrates the results of the computer simulations for the cases of shallow and deep implantation. Figure parts (a) and (d) show the distribution of the implanted ions. The more important distribution of remaining damage is depicted in (b) and (e). These show the value of interstitials minus vacancies, which assumes annihilation of these defects within each simulation cell.

The remaining damage helps us understand the opposite bending of the nanowires for the situation of low and high energy implantation. At low ion energies (figure 3(b)) most of the damage is induced on the side of the NW that faces the incident ion beam. There is a thin layer with excess vacancies very close to the surface of the NW. Considering the sputter yield, this thin vacancy-rich layer is mostly removed directly during the irradiation, but the static computer simulations do not account for this removal. Mostly, the upper part of the NW is filled with excess interstitials. This additional material leads to a volume expansion of the upper part. Since the lower part is unaffected by the ion beam and not expanded, compressive stress occurs on the irradiated side, while tensile stress is induced on the non-irradiated side. Therefore, a bending moment occurs, which bends the NW away from the ion beam.

For the case of high energy implantation, the complete volume of the nanowire is affected by the ion beam (see figure 3(e)). However, in this case an excess of vacancies remains in the part facing the ion beam, while excess interstitials remain in the lower part. The vacancies lead to a volume reduction of the upper part of the nanowire, the interstitials to a volume expansion of the lower part. Together, this induces a bending moment, which bends the nanowire towards the incident ion beam. For high fluences, this leads to an alignment of the nanowire axis with the ion beam, as explained in [16]. Note, in figure 2(c) that there are a few thicker nanowires in the background that are not aligned to the ion beam direction. The reason is that, for thicker nanowires, the ions do not reach the second half and thus no interstitial excess is accumulated on the side facing away from the ion beam. Alignment of all NWs can be achieved only for a diameter distribution which is not too broad.

These results from irradiation of ZnO nanowires corroborate the model we suggested for the bending and alignment of GaAs nanowires [16]. This indicates that the model is not restricted to a particular material system, but may be applicable to many different materials. It should be noted that the GaAs nanowires can be amorphized by ion irradiation [25], while ZnO remains crystalline during irradiation even at very high ion fluences [26]. This raises the question how the crystal structure of the ZnO nanowires is affected by the ion beam irradiation and how the structure accommodates the bending of the nanowires. The ZnO nanowires grow in the *c*-direction, resulting in a parallel alignment of the NW axis and the ZnO [0001]-direction [18]. Transmission electron microscopy (TEM) measurements show that after ion beam irradiation the NW axis is still aligned with the *c*-direction at each point on the bent nanowire. This is illustrated in figure 4(a), which shows an irradiated bent nanowire and three high resolution TEM (HR-TEM) micrographs on different locations of the nanowire. The spacing of the fringes in each HR-TEM image corresponds to the spacing of Zn planes in the *c*-direction of ZnO. At each point the planes are perpendicular to the local nanowire axis, indicating that the NW maintains its crystal orientation with respect to the nanowire axis at each point and the *c*-direction is gradually changing along with the nanowire.

The question arises, how this gradual change of crystal orientation is arranged. To investigate this issue, we consider the tensile/compressive stress in the axial direction induced in the nanowire close to its surfaces due to the bending. For a curvature of 0.5 μm^{-1} and nanowires with 50–100 nm diameter, one obtains 2–4 GPa for the tensile or compressive stress close to the NW surface (considering the

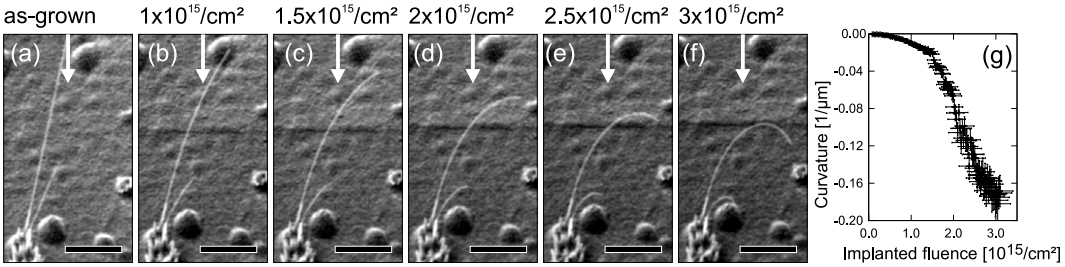

Figure 5. ((a)–(f)) A series of *in situ* SEM images of a single ZnO nanowire irradiated with an increasing fluence of 30 keV Ga ions (low energy situation) in the FIB. Scale bars denote 10 μm, arrows indicate the ion beam direction. (g) Curvature measured as a function of implanted fluence of a single nanowire. Here, error bars denote the inaccuracy of measurement (ca. 10%).

increased Young's modulus for ZnO nanowires as compared to bulk [27]). This is a little below the yield strength of 7.0 GPa [28], which is the limit for elastic bending of ZnO nanowires [29]. However, irradiation with energetic particles is known to enhance the nucleation of dislocation loops under axial strain [30] and dislocation loops have been observed in ion irradiated ZnO [31, 32]: the ion irradiation promotes the nucleation and motion of dislocations by introducing point defects in the material. Since the stress caused by bending is inhomogeneous (it varies from compressive to tensile from one side to the other of the nanowire), the dislocation loops can move, grow and partly be pushed towards the NW surface, leaving behind single edge dislocations. Indeed, dislocations can be found in the irradiated nanowires, as illustrated in figure 4(b), which shows a Fourier-filtered HR-TEM image of the implanted and bent nanowire. The creation and motion of dislocations in the nanowire allow relaxation of the axial stresses. This accounts for a plastic and not just elastic bending of the nanowires, making the bending permanent. This assumption will further be corroborated by results from annealing experiments (see section 3.2).

3.2. Single nanowire irradiation

The results for single nanowire irradiation using the FIB (situation (2A)) are illustrated in figures 5(a)–(f), showing a series of SEM images recorded after irradiation with an increasing fluence of 30 keV Ga^+. Here, the focused ion beam comes from the top (see arrows) and is scanned over an area surrounding the nanowire, resulting in a homogeneous irradiation of the complete nanowire. Initially, the nanowire is straight but inclined to the substrate surface. Under ion irradiation, the nanowire bends away from the ion beam, down towards the substrate surface. This observation of bending away from the ion beam fully supports the results of low energy ensemble irradiation discussed in section 3.1.

However, due to the *in situ* monitoring capabilities when using the FIB, the curvature as a function of ion fluence can be measured for one single nanowire (in contrast to the statistical averages obtained from ensemble irradiation). Furthermore, the *in situ* monitoring accounts for many more data points available, see figure 5(g). These two advantages over ensemble irradiation allow a more detailed analysis of curvature as a function of ion fluence.

For small fluences the absolute value of the curvature increases slowly. However, with increasing fluence, at approximately 1.5×10^{15} ions cm^{-2}, the bending proceeds faster and the slope of curvature as a function of fluence increases. At even higher fluences (above about 2.5×10^{15} ions cm^{-2}), the slope of the curvature decreases again and further bending slows down. This observation can be partly explained by simple geometrical effects: first, the angle between the nanowire axis and the ion beam is small, meaning that the nanowire offers a small cross section to the ion beam and only few ions are implanted per nanowire length. As the nanowire bends away from the ion beam, the angle between the ion beam and the nanowire axis increases (see figure 5(c)) and with that the number of implanted ions per nanowire length. Thus, the bending takes place faster. However, when parts of the nanowire become perpendicular to the ion beam (see figure 5(e)), the projected range of the ions in the nanowire increases. This shifts the defect distribution and, consequently, the volume expansion moves deeper into the nanowire. Thus, the additional bending moment decreases and the bending slows down. The different number of implanted ions per length of bent nanowire also explains why the curvature after irradiation is not homogeneous along the complete nanowire.

This process is enhanced by sputtering: computer simulations show that approximately 7–10 atoms are ejected from the nanowire for each impinging ion. This corresponds to an average reduction of nanowire diameter of approximately 2 nm for a fluence of 2.5×10^{15} ions cm^{-2}. A reduced diameter of the nanowire has the same effect on the bending as an increased projected range.

The changes of the slope of curvature as a function of fluence are not clearly observable for the ensemble irradiation (compare figures 1(e) and 5(g)), due to the larger steps in fluence and the statistical errors in curvature. In the ensemble measurements one can mainly observe a slow increase in curvature, that the single NW irradiation shows above about 2.5×10^{15} ions cm^{-2}.

However, one would not expect ensemble irradiation to yield exactly the same results as single NW irradiation, due to the different ion species: while the noble gas ions are not assumed to change the chemistry of the ZnO nanowires, the implanted Ga ions may destabilize the ZnO compound and change its mechanical properties. Furthermore, in the ensemble irradiation there is the possibility that some nanowires are shadowed by others and suffer fewer ion impacts, thus possibly distorting the average values of curvature.

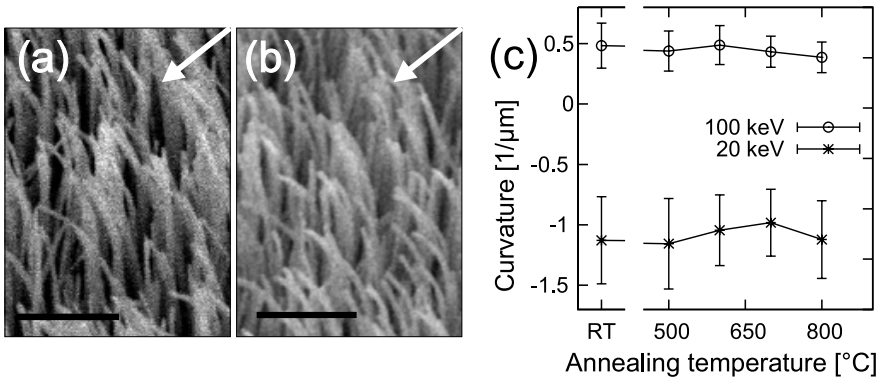

Figure 6. Nanowires bent by irradiation with 3.4×10^{16} ions cm^{-2} of 20 keV Ar ions. SEM images before (a) and after (b) annealing at 800 °C in air for 30 min. Scale bars denote 1 μm. (c) Curvature as a function of annealing temperature for bent nanowires. Nanowires at 'RT' are not annealed.

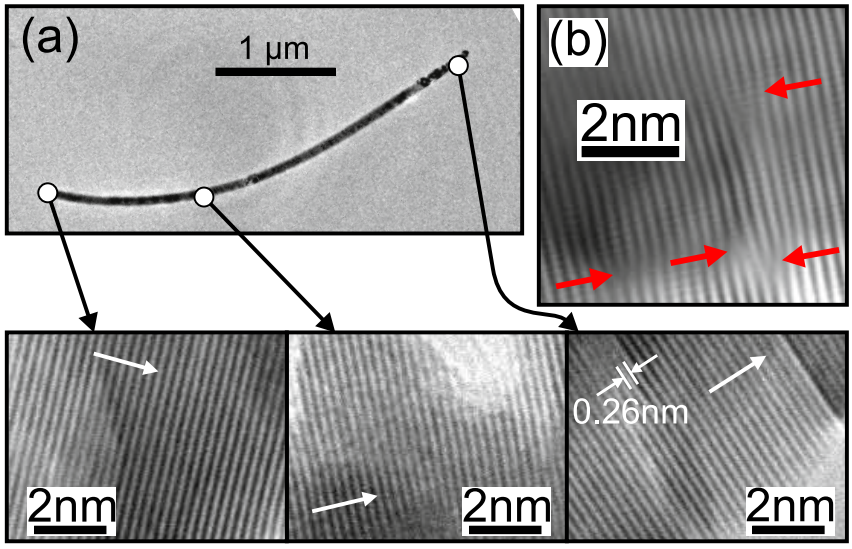

Figure 7. TEM images of a bent nanowire after implantation of 2×10^{16} ions cm^{-2} with 100 keV Ar ions and subsequent annealing at 800 °C. (a) Overview TEM micrograph and three HR-TEM images taken at different points on the nanowire. The line spacing in the HR-TEM micrographs corresponds to the Zn-plane spacing in the *c*-direction indicated by the white arrows. (b) Fourier-filtered HR-TEM image with arrows pointing to dislocations.

3.3. Subsequent annealing

The results from the annealing experiments are illustrated in figure 6, where the SEM images show an ensemble of bent nanowires (after irradiation with 3.4×10^{16} ion cm^{-2} of 20 keV Ar ions) before (a) and after (b) annealing at 800 °C in air at ambient pressure. At 900 °C, the nanowires are observed to decompose, probably due to the reduction of ZnO by carbon, of which a small amount is deposited during ion beam irradiation (results not shown here).

The nanowires are still bent after the annealing at 800°. In order to evaluate the effect of annealing on the bending in detail, the average curvatures of a large number of nanowires were measured for increasing annealing temperatures. This was done for both low- and high energy irradiation. The results are illustrated in figure 6(c). No significant change in the curvatures can be observed. Furthermore, HR-TEM investigations of implanted and annealed nanowires show that the nanowires are still oriented with the *c*-direction along the nanowire axis, see figure 7(a).

It has been reported that extended defects in ZnO are removed during annealing only up to ion fluences of approximately 5×10^{14} ions cm^{-2}, but they persist after implanting with higher fluences and annealing [31, 33, 34]. Removal of most extended defects is expected only for temperatures above 1000 °C [35]. Indeed, Fourier-filtered HR-TEM images of irradiated and annealed nanowires (figure 7(b)) show that dislocations can still be found after annealing at 800 °C. The thermal energy at 800 °C alone (≈0.092 eV) cannot move the dislocations because the activation energy for dislocation motion is around 0.7–1.2 eV in ZnO [36]. However, small values of stress could move dislocations at these temperatures: at 800 °C the yield stress in ZnO is reduced to approximately 20–30 MPa [36]. But since the curvature of the nanowires does not change on annealing, we can conclude that the stress in the bent nanowires is already

mostly relaxed before the annealing. This substantiates our assumption, expressed above, that the nanowire bending by ion irradiation is a plastic deformation.

4. Conclusion

Ion beam irradiation can be used to bend and align ZnO nanowires. Depending on the ion energy, the bending direction can be controlled. The underlying mechanism can be understood by the distribution of ion beam induced damage, at the beginning of the bending namely interstitials and vacancies. These induce compressive and tensile stresses, respectively, leading to a bending moment, which turns into a plastic deformation of ZnO nanowires. This is in contrast to methods using external forces for bending, where the deformation is only elastic and fracture occurs above a strain limit [29]. In ion beam induced bending, the stresses are relaxed by ion beam induced nucleation and motion of dislocations, which makes the bending permanent, even persisting upon annealing up to 800 °C. It should be noted that annealing at these temperatures is known to reduce very many of the ion beam induced point defects in ZnO nanowires, thus enhancing their electrical and optical properties [21, 32].

Since the bending is similar for GaAs nanowires, one might expect that the underlying processes are not distinct for a certain semiconductor material but of a more universal nature.

Acknowledgments

The authors acknowledge funding by the DFG under grant Ro1198/7-3, funding by the European Commission in the FP7, NMP priority of the project FIBLYS and funding by NANOSTRESS, a joint project of the Fraunhofer and MPI societies.

References

[1] Barth S, Hernandez-Ramirez F, Holmes J D and Romano-Rodriguez A 2010 Synthesis and applications of one-dimensional semiconductors *Prog. Mater. Sci.* **55** 563–627

[2] Kim F, Kwan S, Akana J and Yang P 2001 Langmuir–Blodgett nanorod assembly *J. Am. Chem. Soc.* **123** 4360–1

[3] Yu G, Li X, Lieber C M and Cao A 2008 Nanomaterial-incorporated blown bubble films for large-area, aligned nanostructures *J. Mater. Chem.* **18** 728–34

[4] Smith P A, Nordquist C D, Jackson T N, Mayer T S, Martin B R, Mbindyo J and Mallouk T E 2000 Electric-field assisted assembly and alignment of metallic nanowires *Appl. Phys. Lett.* **77** 1399–401

[5] Ronning C, Borschel C, Geburt S and Niepelt R 2010 Ion beam doping of semiconductor nanowires *Mater. Sci. Eng.* R **70** 30

[6] Gehrke H-G, Nix A-K, Hofsäss H, Krauser J, Trautmann C and Weidinger A 2010 Self-aligned nanostructures created by swift heavy ion irradiation *J. Appl. Phys.* **107** 094305

[7] Toma A, Chiappe D, Boragno C and Buatier de Mongeot F 2010 Self-organized ion-beam synthesis of nanowires with broadband plasmonic functionality *Phys. Rev.* B **81** 165436

[8] Cronin S B, Lin Y-M, Rabin O, Black M R, Ying J Y, Dresselhaus M S, Gai P L, Minet J-P and Issi J-P 2002 Making electrical contacts to nanowires with a thick oxide coating *Nanotechnology* **13** 653

[9] Inkson B J, Dehm G and Wagner T 2004 Thermal stability of Ti and Pt nanowires manufactured by Ga^+ focused ion beam *J. Microsc.* **214** 252–60

[10] Gierak J, Madouri A, Bourhis E, Travers L, Lucot D and Harmand J C 2010 Focused gold ions beam for localized epitaxy of semiconductor nanowires *Microelectron. Eng.* **87** 1386–90

[11] Jun K and Jacobson J M 2010 Programmable growth of branched silicon nanowires using a focused ion beam *Nano Lett.* **10** 2777–82

[12] Lee K M, Choi T Y, Lee S K and Poulikakos D 2010 Focused ion beam-assisted manipulation of single and double β-SiC nanowires and their thermal conductivity measurements by the four-point-probe 3-ω method *Nanotechnology* **21** 125301

[13] Romano L, Rudawski N G, Holzworth M R, Jones K S, Choi S G and Picraux S T 2009 Nanoscale manipulation of Ge nanowires by ion irradiation *J. Appl. Phys.* **106** 114316

[14] Jun K, Joo J and Jacobson J M 2009 Focused ion beam-assisted bending of silicon nanowires for complex three-dimensional structures *J. Vac. Sci. Technol.* B **27** 3043–7

[15] Tuboltsev V and Raisanen J 2009 Sculpturing nanowires with ion beams *Small* **5** 2687–91

[16] Borschel C, Niepelt R, Geburt S, Gutsche C, Regolin I, Prost W, Tegude F-J, Stichtenoth D, Schwen D and Ronning C 2009 Alignment of semiconductor nanowires using ion beams *Small* **5** 2576–80

[17] Wagner R S and Ellis W C 1964 Vapor–liquid–solid mechanism of single crystal growth *Appl. Phys. Lett.* **4** 89–90

[18] Borchers C, Müller S, Stichtenoth D, Schwen D and Ronning C 2006 Catalyst-nanostructure interaction in the growth of 1D ZnO nanostructures *J. Phys. Chem.* B **110** 1656–60

[19] Chen Z H, Tang Y B, Liu Y, Yuan G D, Zhang W F, Zapien J A, Bello I, Zhang W J, Lee C S and Lee S T 2009 ZnO nanowire arrays grown on Al:ZnO buffer layers and their enhanced electron field emission *J. Appl. Phys.* **106** 064303

[20] Ronning C *et al* 2010 Tailoring the properties of semiconductor nanowires using ion beams *Phys. Status Solidi* **247** 2329

[21] Geburt S, Stichtenoth D, Müller S, Dewald W, Ronning C, Wang J, Jiao Y, Rao Y Y, Hark S K and Li Q 2008 Rare earth doped zinc oxide nanowires *J. Nanosci. Nanotechnol.* **8** 244–51

[22] Lorenz K, Alves E, Wendler E, Bilani O, Wesch W and Hayes M 2005 Damage formation and annealing at low temperatures in ion implanted ZnO *Appl. Phys. Lett.* **87** 191904

[23] Ziegler J F, Biersack J P and Littmark U 1985 *Stopping and Range of Ions in Solids* (New York: Pergamon)

[24] Borschel C and Ronning C 2011 Ion beam irradiation of 3D nanostructures-a new Monte Carlo simulation code, in preparation, see www.iradina.de

[25] Stichtenoth D, Wegener K, Gutsche C, Regolin I, Tegude F J, Prost W, Seibt M and Ronning C 2008 P-type doping of GaAs nanowires *Appl. Phys. Lett.* **92** 163107

[26] Naguib H M and Kelly R 1975 Criteria for bombardment-induced structural changes in non-metallic solids *Radiat. Eff.* **25** 1–12

[27] Chen C Q, Shi Y, Zhang Y S, Zhu J and Yan Y J 2006 Size dependence of Young's modulus in ZnO nanowires *Phys. Rev. Lett.* **96** 075505

[28] Riaz M, Fulati A, Zhao Q X, Nur O, Willander M and Klason P 2008 Buckling and mechanical instability of ZnO nanorods grown on different substrates under uniaxial compression *Nanotechnology* **19** 415708

[29] Chen C Q and Zhu J 2007 Bending strength and flexibility of ZnO nanowires *Appl. Phys. Lett.* **90** 043105
[30] Heald P T and Speight M V 1974 Steady-state irradiation creep *Phil. Mag.* **29** 1075
[31] Wendler E, Bilani O, Gärtner K, Wesch W, Hayes M, Auret F D, Lorenz K and Alves E 2009 Radiation damage in ZnO ion implanted at 15 K *Nucl. Instrum. Methods* B **267** 2708–11
[32] Weissenberger D, Dürrschnabel M, Gerthsen D, Perez-Willard F, Reiser A, Prinz G M, Feneberg M, Thonke K and Sauer R 2007 Conductivity of single ZnO nanorods after Ga implantation in a focused-ion-beam system *Appl. Phys. Lett.* **91** 132110
[33] Yao L D, Weissenberger D, Dürrschnabel M, Gerthsen D, Tischer I, Wiedenmann M, Feneberg M, Reiser A and Thonke K 2009 Structural and cathodoluminescence properties of ZnO nanorods after Ga-implantation and annealing *J. Appl. Phys.* **105** 103521
[34] Ronning C, Schwen D, Gao P X, Ding Y and Wang Z L 2004 Manganese-doped ZnO nanobelts for spintronics *Appl. Phys. Lett.* **84** 783–5
[35] Kucheyev S O, Williams J S, Jagadish C, Zou J, Evans C, Nelson A J and Hamza A V 2003 Ion-beam-produced structural defects in ZnO *Phys. Rev.* B **67** 094115
[36] Yonenaga I, Ohno Y, Taishi T and Tokumoto Y 2009 Recent knowledge of strength and dislocation mobility in wide band-gap semiconductors *Physica* B **404** 4999–5001